Article

Structure

Structure of Prolyl-tRNA Synthetase-Halofuginone Complex Provides Basis for Development of Drugs against Malaria and Toxoplasmosis

Graphical Abstract

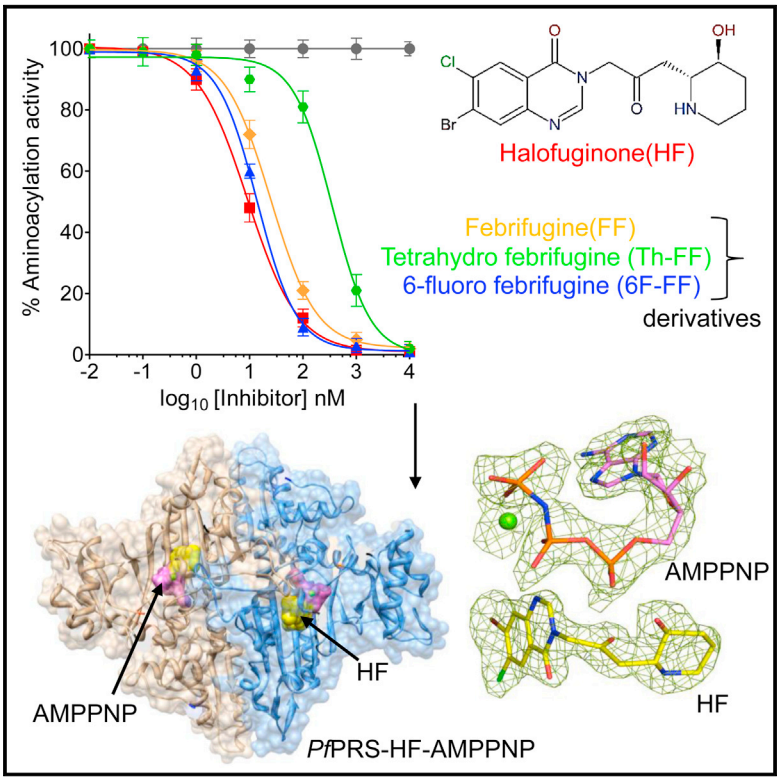

Highlights

- Atomic structure of PfPRS-AMPNP-HF complex to 2.3 Å resolution
- *P. falciparum* growth and PfPRS activity are both inhibited by HF and its derivatives
- *T. gondii* growth is inhibited by HF
- Protein targets for HF-based derivatives are prolyl-tRNA synthetases

Authors

Vitul Jain, Manickam Yogavel, ..., Mohamed-Ali Hakimi, Amit Sharma

Correspondence

amit.icgeb@gmail.com

In Brief

The structure of PfPRS-HF-AMPPNP, described by Jain et al., provides a structural rationale for the killing action of HF-based derivatives of apicomplexan parasites such as *Plasmodium falciparum* and *Toxoplasma gondii*. High-affinity drug binding and high-potency enzyme activity inhibition confirms prolyl-tRNA synthetases as valuable new anti-pathogen targets.

Accession Numbers

4YDQ

Jain et al., 2015, Structure *23*, 819–829
May 5, 2015
http://dx.doi.org/10.1016/j.str.2015.02.011

Structure
Article

Structure of Prolyl-tRNA Synthetase-Halofuginone Complex Provides Basis for Development of Drugs against Malaria and Toxoplasmosis

Vitul Jain,[1] Manickam Yogavel,[1] Yoshiteru Oshima,[2] Haruhisa Kikuchi,[2] Bastien Touquet,[3,4] Mohamed-Ali Hakimi,[3,4] and Amit Sharma[1,*]
[1]Structural and Computational Biology Group, International Centre for Genetic Engineering and Biotechnology (ICGEB), Aruna Asaf Ali Road, New Delhi 110067, India
[2]Laboratory of Natural Product Chemistry, Graduate School of Pharmaceutical Sciences, Tohoku University, Aoba-yama Aoba-ku, Sendai 980-8578, Japan
[3]CNRS, UMR5163, LAPM, 38041 Grenoble, France
[4]Université Joseph Fourier, 38000 Grenoble, France
*Correspondence: amit.icgeb@gmail.com
http://dx.doi.org/10.1016/j.str.2015.02.011

SUMMARY

The Chinese herb *Dichroa febrifuga* has traditionally treated malaria-associated fever. Its active component febrifugine (FF) and derivatives such as halofuginone (HF) are potent anti-malarials. Here, we show that FF-based derivatives arrest parasite growth by direct interaction with and inhibition of the protein translation enzyme prolyl-tRNA synthetase (PRS). Dual administration of inhibitors that target different tRNA synthetases suggests high utility of these drug targets. We reveal the ternary complex structure of PRS-HF and adenosine 5′-(β,γ-imido)triphosphate where the latter facilitates HF integration into the PRS active site. Structural analyses also highlight spaces within the PRS architecture for HF derivatization of its quinazolinone, but not piperidine, moiety. We also show a remarkable ability of HF to kill the related human parasite *Toxoplasma gondii*, suggesting wider HF efficacy against parasitic PRSs. Hence, our cell-, enzyme-, and structure-based data on FF-based inhibitors strengthen the case for their inclusion in anti-malarial and anti-toxoplasmosis drug development efforts.

INTRODUCTION

Plasmodium parasites are the causative agents of malaria, with an estimated 0.5 million deaths annually. Due to increasing incidence of chloroquine and artemisinin resistance, the World Health Organization (WHO) recommends combination chemotherapy for malaria. There is also increased emphasis on establishing drug pipelines that can generate new anti-malarials by using modern and traditional lead compounds. The ancient Chinese herb *Dichroa febrifuga* has been used to treat malaria for many centuries (Koepfli et al., 1947). The active component of this herb is a quinazolinone-type alkaloid called febrifugine (FF) (Coatney et al., 1950). However, owing to its gastrointestinal toxicity, it was derivatized to yield less toxic compounds (Hewitt et al., 1952). Among this new class of derivatives, halofuginone (HF) showed reduced cellular toxicity (Ryley and Betts, 1973).

HF is currently used as a coccidiostat against *Eimeria* (Ryley and Wilson, 1975) and *Cryptosporidium* (Linder et al., 2007) infections. Studies on HF promise utility against scleroderma, cancer, and fibrotic disease (Elkin et al., 1999; Halevy et al., 1996; McGaha et al., 2002; Pines and Nagler, 1998; Pines et al., 2003). Recently, the molecular target of HF in humans was identified as the prolyl-tRNA synthetase (PRS) enzyme (Keller et al., 2012; Son et al., 2013; Zhou et al., 2013), a member of the aminoacyl-tRNA synthetase (aaRS) family. The latter are ancient enzymes responsible for genetic code translation (Ibba and Soll, 2000), which attach amino acids onto cognate tRNAs for protein translation in an aminoacylation reaction. We and others have studied critical cellular processes such as nucleosome assembly and lipid import in the malaria parasites (Chandra et al., 2005; Gill et al., 2009; Navadgi et al., 2006; Sharma and Sharma, 2011; Sharma et al., 2008). However, lack of experimentally verified "hit" compounds has hampered the discovery of potent malaria parasite inhibitors against these protein targets (Chandra et al., 2005; Gill et al., 2009; Navadgi et al., 2006; Sharma and Sharma, 2011; Sharma et al., 2008). Encouragingly, several groups have been investigating the structure-function attributes of aaRSs within malaria parasites (Bhatt et al., 2009, 2011; Istvan et al., 2011; Jackson et al., 2011; Jain et al., 2014; Khan et al., 2011, 2013a, 2013b, 2014; Koh et al., 2012; Pham et al., 2014). Targeting parasitic aaRSs can provide an additional drug component in current multidrug anti-malarial therapy (Bhatt et al., 2009, 2011; Hoepfner et al., 2012; Istvan et al., 2011; Jackson et al., 2011; Jain et al., 2014; Khan et al., 2011, 2013a, 2013b, 2014; Koh et al., 2012; Pham et al., 2014).

Structural studies have previously suggested that in the case of human PRS, HF mimics the enzyme substrates L-Pro and adenine 76 (A76) of tRNA and then binds into their "active site pockets" simultaneously, but with the assistance of ATP (Keller et al., 2012; Son et al., 2013; Zhou et al., 2013). These findings generated intense excitement about the molecular target of HF in *Plasmodium* parasites. We then showed direct and strong

HF binding to the *Plasmodium falciparum* PRS (PfPRS), thus establishing the cellular target of this drug in malaria parasites (Jain et al., 2014). In the past two decades, many synthetic derivatives of FF and HF have been reported with potent anti-malarial activity (Kikuchi et al., 2006, 2014), and it is very likely that these compounds work by targeting the malaria protein translation machinery by inhibition of the PRS.

Here, we investigate racemic mixtures of quinazolinone-based compounds, namely halofuginone (HF), febrifugine (FF), 6-fluoro febrifugine (6F-FF), and tetrahydro quinazolinone febrifugine (Th-FF), using crystallography, cell- and enzyme-based drug interaction assays. We show their differential utility against malaria parasites, and present a structural basis for their interaction with the PfPRS enzyme. The atomic structure of the ternary complex of PfPRS-halofuginone (PfPRS-HF) in complex with adenosine 5′-(β,γ-imido)triphosphate (AMPPNP) reveals intricacies of drug binding, and suggests chemical spaces available for further drug derivatization. Our dual drug inhibition study on malaria parasites using HF and cladosporin (a *P. falciparum* lysyl-tRNA synthetase [PfKRS] inhibitor) (Hoepfner et al., 2012; Khan et al., 2013a, 2014) validates the *Plasmodium* tRNA synthetase family as valuable new targets for drug development. There is high conservation in HF chelating residues in many pathogen PRSs; based on this we tested HF against *Toxoplasma* parasites. We show very high potency inhibition of *Toxoplasma* parasite growth by HF, thus establishing these quinazolinone-based compounds as general anti-apicomplexan compounds. Our comprehensive analyses provide a platform for focusing on PRS as a new target for the development of novel malaria and toxoplasmosis intervention strategies.

RESULTS

Evaluation of PRS-Drug Binding and Inhibition

We performed cell- and enzyme-based inhibition assays to address drug-like properties of the four quinazolinone-based compounds HF, FF, 6F-FF, and Th-FF (Figure 1; Figure S1). The 3D7 strain of *P. falciparum* was tested for effects of these inhibitors after 48 hr of incubation in concentration ranges of 0.01 nM to 10 μM for each. The drugs HF, FF, 6F-FF, and Th-FF killed malaria parasites in the very first cycle of erythrocytic development, suggesting that the likely target for these inhibitors was cytoplasmic PfPRS and not apicoplastic PfPRS (Hoen et al., 2013). For each of the four tested inhibitors (Figure 1A), dose-dependent inhibition followed sigmoidal curves with 50% effective concentration (EC_{50}) in the subnanomolar ranges of 1–190 nM (Figure 1B), consistent with earlier reports (Derbyshire et al., 2012; Geary et al., 1983; Kikuchi et al., 2006, 2014). The EC_{50} values of HF were increased to 5 and 20 nM, respectively, in the presence of 5× and 20× L-Pro (RPMI media supplemented with higher L-Pro concentration) in the culture media, in line with a competitive inhibition mode of binding in context of the PRS natural substrate L-proline (Figure 1B). To investigate whether HF, FF, 6F-FF, and Th-FF were specific for PfPRS, and would thereby abrogate protein synthesis by inhibiting the enzyme directly, we performed aminoacylation assays in the presence of these drugs (Figure 1C). Our recombinant PfPRS efficiently catalyzed aminoacylation reactions (Figure 1D), which were quantitatively measured by the amount of pyrophosphate released and then estimated using standard curves. For enzyme inhibition studies, concentration ranges of 0.01 nM to 10 μM were used for the four compounds, and inhibitions were assessed in dose-dependent fashion. These revealed 50% inhibitory concentration (IC_{50}) values of 9, 24, 13, and 352 nM, respectively, for HF, FF, 6F-FF, and Th-FF (Figure 1D). We also investigated the binding of HF, FF, 6F-FF, and Th-FF with PfPRS in thermal shift assays (Figure 1E). The profile of PfPRS alone (apo) gave a melting temperature (T_m) of ~50°C at which the ratio of unfolded to folded protein was 1 (Figure 1E). Addition of 6F-FF, Th-FF, and FF individually to PfPRS did not alter the PfPRS thermal profile substantially (small changes of ~0.5°C to 1.5°C in T_m were observed). This was in contrast to the PfPRS-apo interaction with HF, which produced a significant rise of 15°C in enzyme T_m (Figure 1E). However, the addition of ATP analog AMPPNP along with Th-FF, FF, 6F-FF, and HF inhibitors resulted in a substantial T_m shift of ~30°C to 40°C, indicating specificity, higher affinity, and greater stability of PfPRS-inhibitor-AMPPNP complexes (Figure 1E). To estimate the relative binding affinities of HF and AMPPNP for PfPRS, we also performed concentration-dependent thermal shift assays. Binding constants (K_d) were estimated by examining the systematic effect of increasing HF concentration on PfPRS stability (Figure 1F). A concentration range of 0.01 nM to 10 μM was used for HF, while AMPPNP was used at a constant concentration of 1 mM (Figure 1F). The K_d of PRS-HF was estimated as ~300 nM, and interestingly the PfPRS-HF binding affinity increased ~30-fold in the presence of AMPPNP to ~9 nM (Figure 1F). In addition, we performed isothermal titration calorimetry (ITC) experiments (Figure S1) to determine the K_d of HF for PRS-AMPPNP complex. These data reveal value of ~19 nM, similar to those obtained from our thermal shift assay (TSA) experiments (~9 nM). These data together reveal that HF binding to PfPRS is promoted in the presence of AMPPNP, consistent with earlier data on human PRS (Zhou et al., 2013). The drug binding assays (TSA and ITC) and aminoacylation inhibition data together suggest strong and specific interaction between PfPRS and compounds HF, FF, 6F-FF, and Th-FF.

Structure of PfPRS-HF-AMPPNP Complex and Comparison with Human PRS

To dissect the structural basis of inhibitor selectivity by PfPRS and the apparent increase in drug affinity in presence of AMPPNP, we attempted co-crystallization of PfPRS with HF, FF, 6F-FF, and Th-FF. We succeeded in growing crystals of PfPRS in complex with HF and AMPPNP. The crystals were in the monoclinic space group ($P2_1$) where the asymmetric unit contained one dimer of PfPRS-HF-AMPPNP with a solvent content of ~56%. The structure was solved at 2.3 Å resolution by molecular replacement method using PfPRS-apo (PDB code 4TWA) as a search model (Figure 2A). The organization and overall fold of PfPRS ternary complex is similar to that in our earlier report of PfPRS-apo structure (root-mean-square deviation [RMSD] is 0.6 Å for 475 Cα atoms) (Jain et al., 2014). PfPRS shares ~54% identity with human PRS and yielded an RMSD of 1.3 Å for 470 Cα atoms, with limited deviations in AB binding and Z domains only (Figure 2B). In our PfPRS-HF-AMPPNP structure, we observed clear electron densities for the two protomers except for tRNA recognition residues 327–334 and motif 1 residues

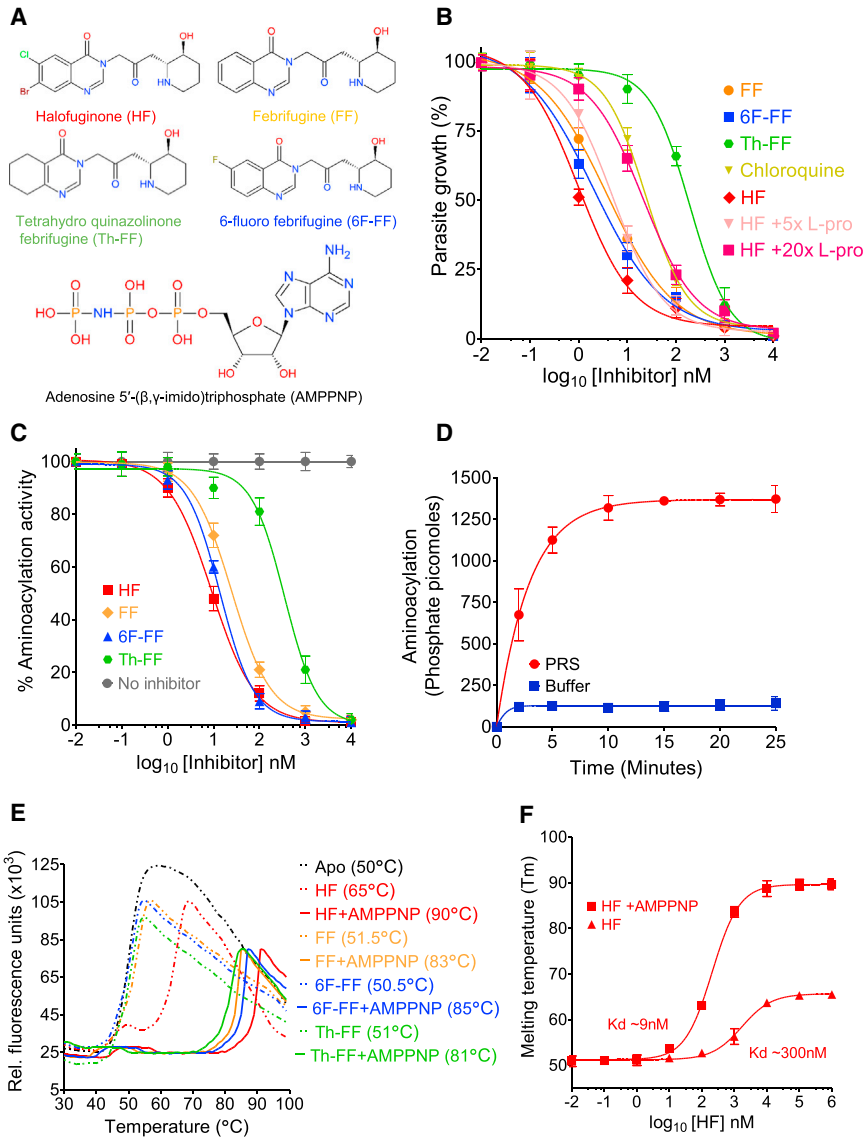

Figure 1. Binding and Inhibition of PfPRS

(A) Chemical structures of halofuginone (HF), febrifugine (FF), 6-fluoro febrifugine (6F-FF), tetrahydro quinazolinone febrifugine (Th-FF), and the ATP analog (adenosine 5′-(β,γ-imido)triphosphate, AMPPNP). The color used for the compound names corresponds to the curve color used for the rest of the graphs.

(B) Parasite growth inhibition assays in the presence of HF, FF, 6F-FF, and Th-FF. The experiments were performed at seven concentrations ranging from 0.1 nM to 10 μM. The EC_{50} values are the mean ± SD (n = 3) nM and are as follows: 1 ± 0.3 for HF; 2 ± 0.5 for 6F-FF; 4 ± 0.6 for FF; 192 ± 4.3 for Th-FF; 24 ± 2.1 for chloroquine; 5 ± 1.1 for HF with 5× L-Pro; and 21 ± 1.0 for HF with 20× L-Pro.

(C) Aminoacylation assays in the presence of HF, FF, 6F-FF, and Th-FF. These experiments were performed at seven concentrations ranging from 0.1 nM to 10 μM. The IC_{50} values are the mean ± SD (n = 3) nM and are as follows: 9 ± 0.6 for HF (red); 13 ± 1.5 for 6F-FF (blue); 24 ± 1.7 for FF (yellow); and 352 ± 17.2 for Th-FF (green).

(D) Aminoacylation activity assays using recombinant PfPRS. Data represent dependence of PO_4^{2-} formation versus time. Two moles of PO_4^{2-} are formed for every mole of $tRNA^{Pro}$ that is acylated. Aminoacylation curves with (blue line) and without (red line) added PfPRS and $tRNA^{Pro}$. Serial dilutions of PO_4^{2-} in reaction buffer were incubated with malachite green solution and the absorbance was measured at 621 nm.

(E) Thermal shift assays with HF, FF, 6F-FF, and Th-FF inhibitors. The inhibitors bind PfPRS in the absence of AMPPNP but interact more strongly in its presence.

(F) Dose-dependent thermal melting curves of PfPRS in the presence of HF with AMPPNP. Values shown are the mean (n = 3). The binding affinity of HF alone and HF with AMPPNP, calculated using the melting profile (Matulis et al., 2005), was ~9 nM and ~300 nM, respectively. See also Figure S1.

697–707; however, a larger overall B factor was observed for molecule B (49 $Å^2$) when compared with molecule A (39 $Å^2$) (Figure 2B). Superposition of PfPRS catalytic domains on *Homo sapiens* PRS (HsPRS) (PDB 4HVC) showed that the conformation and location of bound AMPPNPs and HFs in each protomer are identical (Figure 2B). The ligands HF and AMPPNP were found in their respective pockets with well-defined electron densities (Figure 2C). In both PfPRS and HsPRS, AMPPNP was located in the canonical ATP binding pocket and was stabilized by several hydrogen bonds, water molecules, and hydrophobic contacts (Figure 2B). However, a significant deviation was observed for the terminal phosphate group of AMPPNP in PfPRS when compared with the ligand bound HsPRS (Figures 2D and 2E). In PfPRS, the adenosine ring of AMPPNP stacks between Phe405 and Arg514, and the ribose moiety forms hydrogen bonds with Gln475, Arg514, Thr478, and a water molecule, while Arg390 stabilizes phosphates, Lys384, Arg401, and water ensconced Mg^{2+} (Figures 3A and 3B). Furthermore, in both HsPRS and PfPRS, the α-phosphate group of AMPPNP is proximal to HF and forms hydrogen bonds with the hydroxyl group of HF piperidine ring along with its keto group (Figure 3B). The extensive hydrophilic and hydrophobic interactions position the AMPPNP in a bent conformation in both HsPRS and PfPRS (Figures 3A and 3B). However, the residue Thr478 forms a hydrogen bond with the piperidine ring hydroxyl of HF in PfPRS but not in HsPRS (Figure 3A). From the electron density analysis of Thr478 (Figure 3A), it is evident that its side chain adopts alternate conformations, thereby permitting its hydroxyl group to bond hydrogen with the hydroxypiperidine of HF. The refined occupancies of major and minor conformations of Thr478 are 0.56/0.46 and 0.67/0.33 for molecules A and B, respectively. Thus, Thr478 makes hydrogen bonds to both HF and AMPPNP via major and minor conformations, respectively. The occupancies of bound ligands HF/AMPPNP (0.96/0.91 and 0.92/0.88 for molecules A and B, respectively) were also refined and indicate fully ligand bound states. However, the equivalent residue Thr1240 in

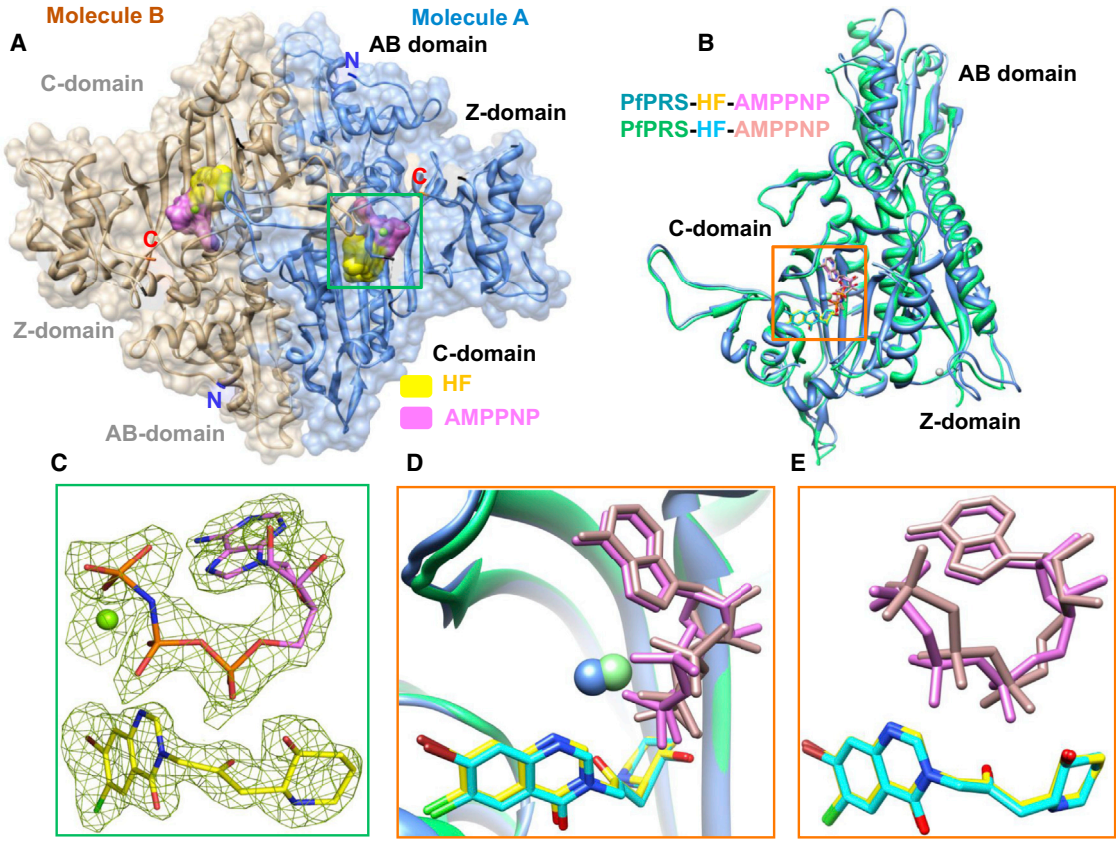

Figure 2. Crystal Structure of the PfPRS-HF-AMPPNP Ternary Complex

(A) PfPRS dimer in the asymmetric unit of PfKRS-HF-AMPPNP crystals is shown with bound HF (yellow) and AMPPNP (pink). Catalytic (C domain, residues 255–532), anti-codon binding (AB domain, residues 533–655), C-terminal zinc binding like (Z domain, residues 656–746) domains as well as protein termini are marked.

(B) Superposition of PfPRS-HF-AMPPNP (blue) and HsPRS-HF-AMPPNP (green) structures. HF and AMPPNP, and Mg^{2+} and Zn^{2+} ions are shown as sticks and spheres, respectively.

(C) A simulated annealing composite omit map generated to 2.3 Å resolution contoured at 1.2σ showing the bound ligands HF (yellow), AMPPNP (pink), and Mg^{2+} (green).

(D and E) Two views showing the tight binding of HF and AMPPNP, and the conformational deviation of three phosphate groups between human and *Plasmodium* PRSs. The color codes are the same as in Figure 1B.

HsPRS-HF-AMPPNP complex does not make contact with HF (Zhou et al., 2013).

Although we used a racemic mixture of HF (commercial source), it is evident from the structure of PfPRS-HF-AMPPNP complex that the bound compound is the 2*R*,3*S*-(+) enantiomer of HF (7-bromo-6-chloro-3-[3-[hydroxy-2-piperidinyl]-2-oxo-propyl]-4-quinazolinone) (Figure 2C). In PfPRS, the N atom of the HF piperidine ring forms hydrogen bonds with Thr359 and Glu361, and the quinazolinone ring is mainly stabilized by hydrophobic interactions, particularly by hydrophobic stacking contacts and interactions of AMPPNP phosphate groups. These intimate interactions thus provide a direction to the binding pose of HF (Figure 4A). Interestingly, water molecule interactions around HF and AMPPNP are different between PfPRS and HsPRS structures (Figure 3B). The bromine and chlorine atoms of HF interact with hydrophobic residues and water molecules, respectively (Figure 4C). The bromine links with the main-chain carbonyl O atom of Phe335 and is completely surrounded by hydrophobic stem of Glu338 and Val339, leaving no space for further additive modifications. In contrast, the chloride hydrogen bonds with two waters and is mostly solvent exposed, thus spatially potentiating additional modifications or derivatization (Figure 4C). The HF piperidine ring, in contrast again, is fully surrounded by the proline binding residues with no empty spaces (Figure 4C). Hence, efforts at derivatization of FF via its halogenated positions can focus around the chlorine position.

Active Site Conservation in Pathogen PRSs and Targeting Dual aaRSs

The architectures of class II synthetase active sites have remained largely conserved over the course of evolution. Therefore, we considered whether HF could potentially kill related human parasites such as *Toxoplasma* spp., among others (Figure 4D). Indeed, we found invariance in all critical HF binding residues in PRSs from the human pathogens analyzed (Figure 4D). We thus conjectured that HF may kill *Toxoplasma* parasites via mechanisms similar to those described above. Propelled by these observations, we assessed the effect of HF on the growth of *Toxoplasma gondii* in human primary foreskin fibroblasts (Figure 5A). The compound HF inhibited *T. gondii* intracellular growth

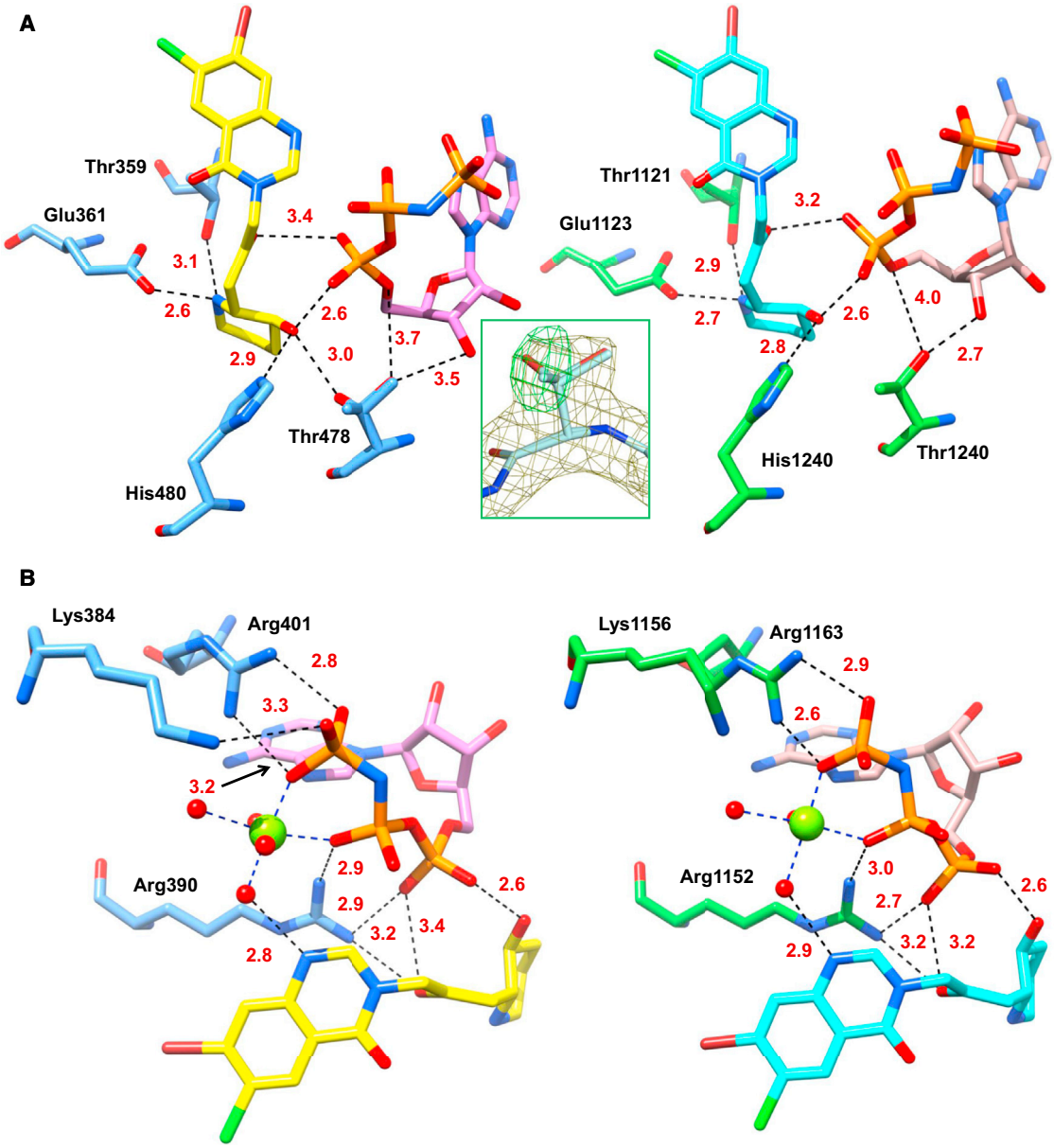

Figure 3. Structural Basis for AMPPNP-Dependent Inhibition of PfPRS by Halofuginone

(A) Important interactions between HF piperidine ring with α-phosphate atoms of AMPPNP and protein residues in PfPRS (left) and HsPRS (right) are shown. The interactions are shown by dashed lines and the distances are marked. The inset mFo-DFc (3.5σ level) and 2mFo-DFc (1.5σ level) electron densities display the alternative conformations of Thr478 in PfPRS. The color codes of the ligands and protein residues are the same as in Figure 2B. The Mg^{2+} ion (green) and water molecules (red) are shown as spheres.

(B) The γ-phosphate group of AMPPNP forms several hydrogen bonding interactions with protein residues, HF, and water molecules, and forms a coordination bond with Mg^{2+}.

at exceedingly low nanomolar concentrations (EC_{50} ~0.94 nM; Figure 5A). It is noteworthy that halofuginone was more effective in inhibiting *T. gondii* growth in a 24 hr assay than the known potent drug pyrimethamine (EC_{50} = 650 nM; Figure 5A), a compound currently used clinically. Using high-content imaging (HCI) assays, we monitored *T. gondii* invasion and growth over a 24 hr period during which it was evident that HF killed *Toxoplasma* faster than the clinical drug pyrimethamine, displaying its higher potency. While HF clearly stops endodyogeny at low concentrations (Figure 5B), it is able to partially prevent invasion when parasites are pretreated with a higher concentration (50 nM; Figure 5C). These data and insights are consistent with the commercially validated utility of HF as a coccidiostat for *Eimeria* and cryptosporidium infections (Linder et al., 2007; Ryley and Wilson, 1975), from which we now predict that HF acts via inhibition of PRS enzyme.

The blooming of the tRNA synthetase family as worthy drug targets in the context of anti-apicomplexan drug discovery is

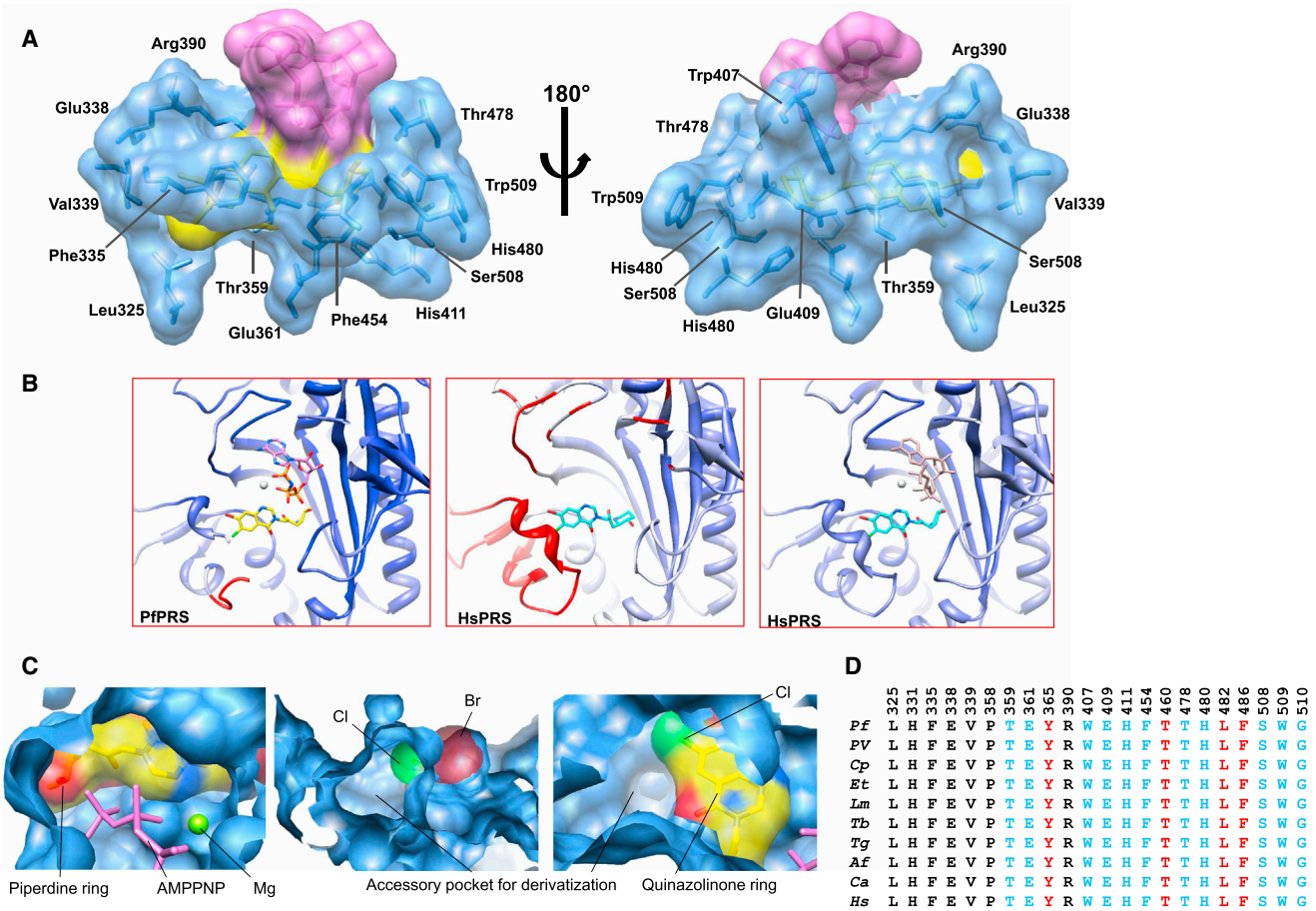

Figure 4. Important HF Binding Pocket Residues

(A) Two views showing the important HF binding pocket residues within 5 Å. Protein residues are shown in stick representations with a transparent overlay of the corresponding Van der Waals surface.

(B) Temperature factor distribution around the active site of PfPRS and HsPRS structures from low (blue) to high (red).

(C) Views of the HF binding pocket. The halogen atoms of HF make interactions within the PRS active site pocket and fill the whole cavity. The hydroxypiperidine ring and the Br site are enclosed in very tight spaces within the enzyme. An accessory pocket is observed near the HF chloride atom and the keto group of 4-quinazoline. Non-halogenated derivatives of FF or partially halogenated ones (such as 6F-FF) are most likely deficient in fully occupying active site cavities within PfPRS.

(D) Multiple sequence alignment of likely HF binding site residues (blue) from various pathogenic PRSs: *Plasmodium falciparum* (Pf), *Plasmodium vivax* (Pv), *Cryptosporidium parvum* (Cp), *Eimeria tenella* (Et), *Leishmania major* (Lm), *Toxoplasma gondii* (Tg), *Trypanosoma brucei* (Tb), *Candida albicans* (Ca), and *Aspergillus flavus* (Af) along with *Homo sapiens* (Hs). The important secondary shell residues are colored red.

highly encouraging. In malaria alone, lead development based on the natural products cladosporin (CL, targets lysyl-tRNA synthetase [KRS]) and FF / HF (target PRS) is ongoing. Hence, we decided to test the effects of co-administration of CL and HF on parasite growth. HF was used at 1 nM and CL at 48 nM so as to cause ~50% reduction in malaria parasite growth (Figure 6A). This level of growth inhibition (EC_{50}) was used to determine, using isobologram analysis, whether the interaction between the two drugs exhibited a synergistic or additive antimalarial effect. The data indicated that the drug combination was indeed additive in all ratios tested (Figure 6A).

DISCUSSION

The 36-member *P. falciparum* parasite tRNA synthetase family, which together governs transmission of genetic information into proteins, has been focus of intense research lately (Bhatt et al., 2009, 2011; Istvan et al., 2011; Jackson et al., 2011; Jain et al., 2014; Khan et al., 2011, 2013a, 2013b, 2014; Koh et al., 2012; Pham et al., 2014). The recent discovery and validation of cladosporin utility against multiple malaria parasitic stages, and its specificity for PfKRS, has been a seminal contribution in validating aaRSs as new drug targets (Hoepfner et al., 2012; Khan et al., 2013a, 2014). Cladosporin is composed of a THP ring (2,6-disubstituted tetrahydropyran) fused to an isocoumarin moiety, and mimics ribose and adenine moieties of the natural substrate ATP, resulting in a scaffold capable of competitive inhibition (Hoepfner et al., 2012; Khan et al., 2013a, 2014). Cladosporin inhibits the malaria parasite with an EC_{50} of ~48 nM; however, its poor bioavailability (ADME [absorption, distribution, metabolism, and excretion] properties) is a hurdle, and hence its derivatization is under way.

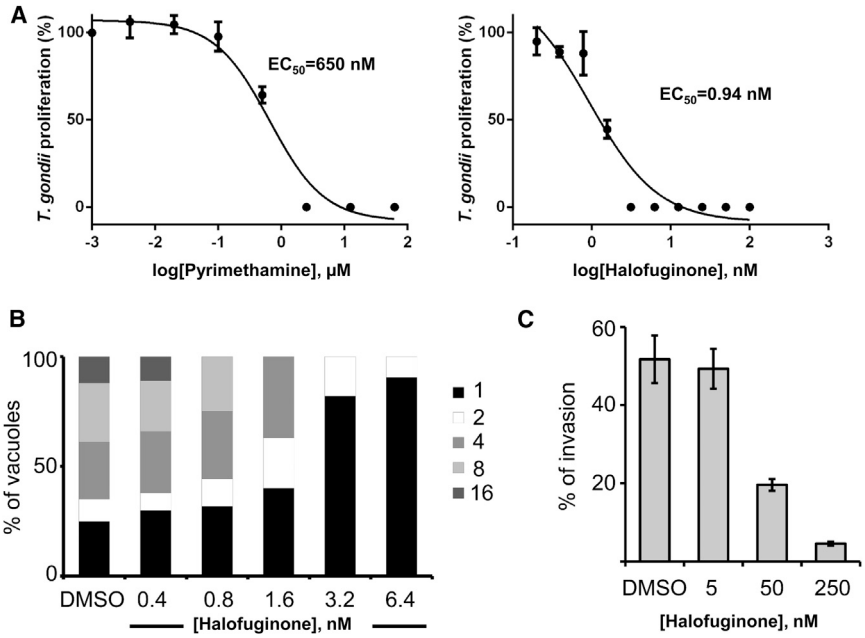

Figure 5. Effect of HF on *T. gondii*

(A) EC_{50} values against *T. gondii* RH tachyzoites were plotted for the clinically relevant compound pyrimethamine and for halofuginone.

(B) Numbers of parasites per vacuole (1, 2, 4, 8, or 16) were counted 24 hr after DMSO (vehicle) or halofuginone treatments.

(C) Parasite invasion was monitored following DMSO (vehicle) or halofuginone treatments.

Another natural product isolated from a Chinese herb, FF, and its halogenated derivative, HF, have shown promising potency as anti-malarials (Hewitt et al., 1952; Derbyshire et al., 2012) and as a veterinary coccidiostat (Linder et al., 2007; Ryley and Wilson, 1975). HF is being explored as therapy for scleroderma, cancer, and fibrotic disease (Elkin et al., 1999; Halevy et al., 1996; McGaha et al., 2002; Pines and Nagler, 1998; Pines et al., 2003). HF is composed of a quinazolinone ring fused to hydroxypiperidine ring and these respectively mimic the natural substrates adenine (3′ tRNA A76) and L-proline, resulting in a PRS dual-site inhibition with assistance from ATP (Son et al., 2013; Zhou et al., 2013). Recently, we have shown direct binding of HF to PfPRS (Jain et al., 2014).

Here, using assays for malaria parasite growth and enzyme inhibition, we demonstrate drug-like utilities of FF and its derivatives (HF, 6F-FF, and Th-FF; Table 1). Intriguingly, the thermal shift profiles indicated that all four compounds interacted with PfPRS in the presence of AMPPNP. Among the four compounds in the presence of AMPPNP, halogenated FF derivatives conferred higher thermal stability than non-halogenated ones (FF and Th-FF). Uniquely, of all four, only HF was able to confer a ~15°C T_m shift with PfPRS alone. The measured binding affinity of HF with PfPRS in the presence of AMPPNP through melting curve analysis (TSA) was ~9 nM, consistent with the ITC data (~19 nM; Figure 1E; Figure S1). The observed inhibition values for HF and 6F-FF (metabolically vulnerable aromatic protons substituted with halogen atoms) suggest that additional halogen(s) increases the potency and activity of FF derivatives. We propose that derivatization of FF via its chlorine position may be feasible from a structural perspective in search of lead molecules.

The substrate binding pockets in PfPRS and HsPRS are highly conserved (Son et al., 2013; Zhou et al., 2013). Our sequence and structure-based exploration of related pathogen PRSs reveals conservation in the HF interacting residues within PRS active sites. Hence, HF-like compounds may be of much wider utility in drug development efforts that target pathogen PRSs. These predictions are validated by our data on HF-mediated killing of *Toxoplasma* parasites. We also tested whether dual anti-tRNA synthetase inhibitors can be useful in combination. For this, we used KRS and PRS inhibitors (cladosporin and HF) simultaneously on *P. falciparum* parasites, revealing additive inhibitory effects on growth. It is noteworthy that the binding sites and mechanism of action of cladosporin and HF are different (Figure 6B). In summary, our work substantiates and directs focus on exploitation of HF-based leads for the generation of specific and effective therapeutics against human and animal pathogens.

EXPERIMENTAL PROCEDURES

P. falciparum Culture

P. falciparum 3D7 was cultured in O^+ erythrocytes in RPMI 1640 (Invitrogen) supplemented with 4.5 mg ml^{-1} glucose (Sigma), 0.1 mM hypoxanthine (Invitrogen), 25 mg ml^{-1} gentamicin (Invitrogen), and 0.5% AlbuMax-I (Invitrogen), according to standard methods (Trager and Jensen, 2005). Parasites were sorbitol treated in ring stages to maintain a synchronized culture as described by Tonkin et al. (2004).

P. falciparum Growth Inhibition Assays

HF was dissolved in DMSO (Sigma) while FF, 6F-FF, and Th-FF were dissolved in double-distilled water. The 3D7 strain of *P. falciparum* was cultured in 96-well plates and synchronized at ring stages. At ~1% parasitemia and 4% hematocrit, HF, FF, 6F-FF, and Th-FF from 0.01 nM to 10 μM were incubated for 48 hr with the parasite culture. Parasite growth was assayed by the SYBR green I (Molecular Probes) DNA staining assay as described earlier (Smilkstein et al., 2004). In brief, 100 μl of SYBR green dye in 1× concentration in lysis buffer supplemented with 0.1% saponin was added to each well. After 45 min incubation at 37°C, fluorescence was estimated using a multiwell plate reader (Victor 3, Perkin Elmer) with excitation and emission wavelength bands centered at 485 and 530 nm, respectively. Chloroquine was taken as a positive control and all experiments were performed in triplicate. For competition experiments with L-proline, this was added to the culture during the assays. The EC_{50} values were obtained by plotting fluorescence values expressed in terms of percentage inhibition of parasite growth at each inhibitor concentration. Analysis was done using non-linear regression analysis with GraphPad Prism 5 software. All data are shown for three replicates as the mean ± SE.

Protein Purification and Thermal Shift Assays

PfPRS was produced in accordance with methods published (Jain et al., 2014). TSAs for PfPRS in the presence of HF, FF, 6F-FF, and Th-FF were performed as reported earlier (Jain et al., 2014). For dose-dependent TSA, PfPRS was diluted in buffer containing 50 mM HEPES (pH 7.5), 300 mM NaCl, and

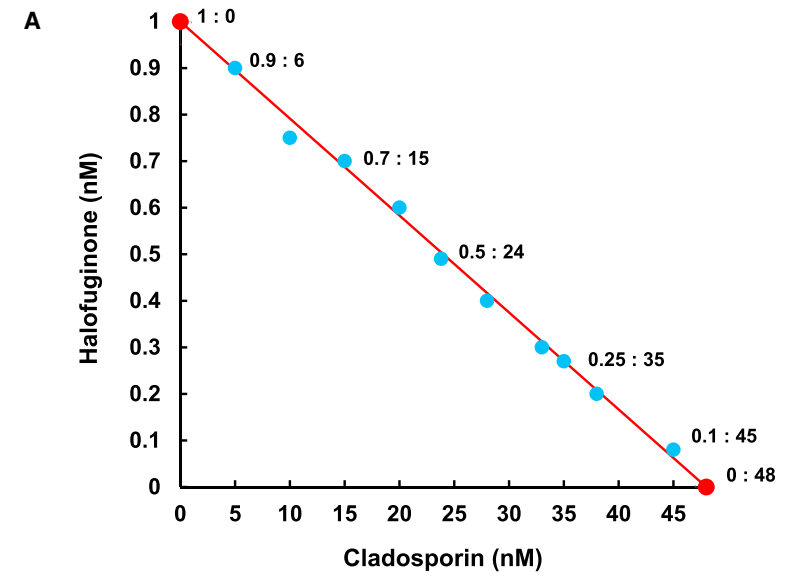

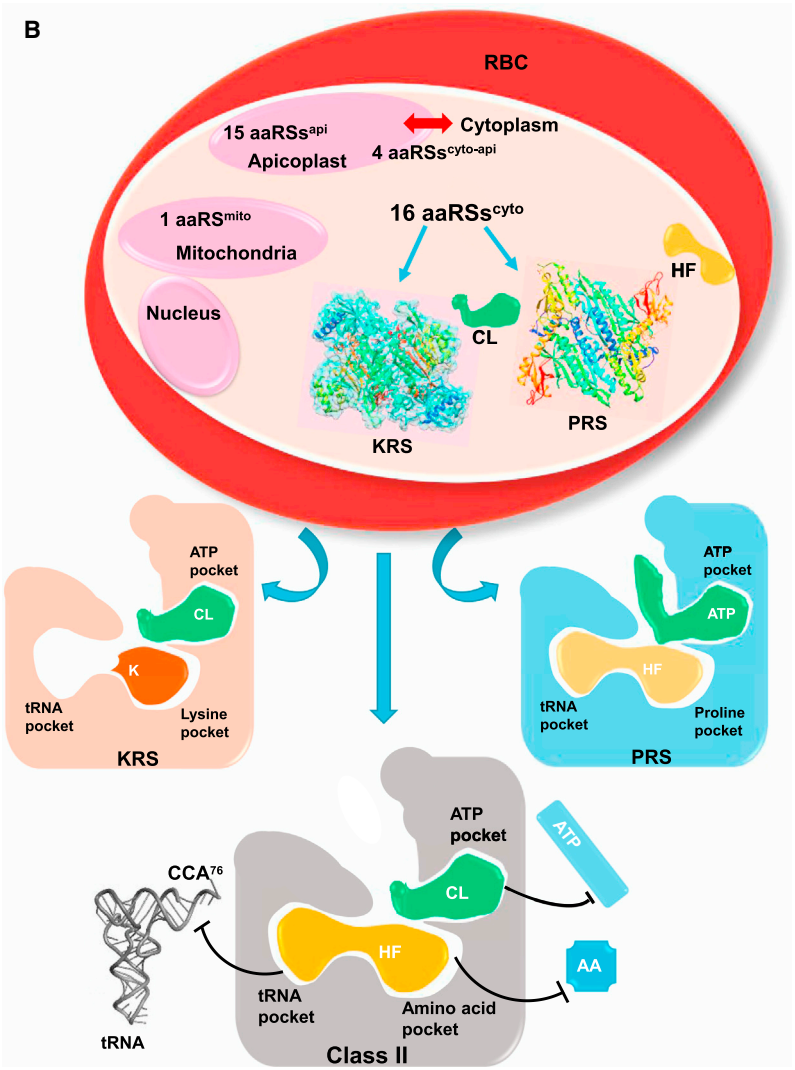

Figure 6. Drug Combination Study

(A) Isobologram demonstrating the additive action of CL and HF on 3D7 parasites. HF at 1 nM and CL at 48 nM were added alone to the culture, which reduced the parasite growth to ~50% (red line). The experimental data points show the ratios of drug combinations (red for drugs used alone and blue for both drugs) that give 50% inhibition in parasite growth.

(B) Summary of tRNA synthetase localizations and drug targeting to date. HF is an ATP-dependent dual-site inhibitor of PRS as it occupies both the proline binding and the 3′ $tRNA^{Pro}$ pocket. CL is known to interact with the ATP binding residues of PfKRS. Using HF and CL in combination will thus be targeting two different enzymes simultaneously, increasing the potency of inhibition via abrogating protein translation in the parasites. The upper figure shows the localization data on 36 *P. falciparum* aaRSs within blood-stage red blood cells (RBCs) in different parasite compartments. PRS and KRS are shown in ribbon diagrams based on their crystal structures in complex with the drugs. The cartoon represents data on class II synthetases that are so far validated via the use of HF and CL.

Table 1. Summary of the Inhibition and T_m Values of Tested Inhibitors in *Plasmodium falciparum*

S. No.	Inhibitor	Enzyme Inhibition IC_{50} (nM)	Parasite (3D7) Inhibition EC_{50} (nM)	Change in Melting Temperature ΔT_m (°C)		Mammalian Cells EC_{50} (nM)	Selectivity Index
				Only Drug	Drug with AMPPNP		
1	HF	9 ± 0.6	1 ± 0.3	15 ± 0.6	40 ± 0.7	150 ± 9[a]	150
2	FF	24 ± 1.7	4 ± 0.6	1.5 ± 0.2	33 ± 0.5	450 ± 20[b]	118
3	6F-FF	13 ± 1.5	2 ± 0.5	0.5 ± 0.1	35 ± 0.5	205 ± 12[b]	108
4	Th-FF	352 ± 7.2	192 ± 4.3	1 ± 0.1	31 ± 0.4	190000 ± 1100[c]	934

[a]Keller et al., 2012.
[b]Kikuchi et al., 2006.
[c]Kikuchi et al., 2014.

2× SYPRO orange dye (Life Technologies). HF (Sigma) at concentrations ranging from 0.1 nM to 1 mM with and without AMPPNP (Sigma) at 1 mM were added to PfPRS (3 μM) and incubated at room temperature for 10 min. PfPRS-apo and with various drugs were heated from 25°C to 99°C at a rate of 1°C min^{-1} and fluorescence signals were monitored by the StepOne Plus quantitative real-time PCR system (Life Technologies). Each curve is an average of three measurements, and data were analyzed using Thermal Shift software (Life Technologies). Inhibitors and AMPPNP alone in assay buffers, with no protein controls, were used, and flat lines were observed for these fluorescence readings at all temperatures. Derivative T_m was used for analysis. Binding constant calculations were done as reported earlier (Matulis et al., 2005).

Crystallization

Highly pure protein was stored in 15 mM HEPES (pH 7.5), 200 mM NaCl, and 10 mM β-mercaptoethanol at 193 K. Before crystallization, 3 mM HF and 5 mM AMPPNP were added to protein and incubated at 4 °C for 10 min. Crystallization was achieved using a vapor diffusion method in hanging drops. A TTP Labtech Mosquito robot was employed to mix 100 nl of PfPRS-AMPPNP-HF complex with 100 nl of well solutions from commercially available crystal screens. Diffraction-quality crystals were obtained with the well solution 0.1 M Bis-Tris (pH 6.5), 2 % (v/v) Tacsimate (pH 5.0), and 12% (w/v) polyethylene glycol 3350.

Aminoacylation Assays

cDNA oligonucleotides were purchased from Sigma with one containing the T7 RNA polymerase promoter followed by gene encoding the $tRNA^{pro}$ while the other primer encoded the complementary strand with promoter and the tRNA gene. These two oligos were mixed in equimolar ratios in an annealing buffer (10 mM Tris [pH 8.0], 50 mM NaCl, and 0.5 mM EDTA), heated to 95°C and then cooled slowly at room temperature. The annealed dsDNA was used as template for in vitro transcription reaction to produce $tRNA^{pro}$, performed using the Ambion Maxiscript T7 in vitro transcription kit. The enzymatic assays were done according to an earlier report (Cestari and Stuart, 2013) where the standard aminoacylation reaction ingredients were aminoacylation buffer (30 mM HEPES [pH 7.4], 140 mM NaCl, 30 mM KCl, and 40 mM $MgCl_2$), 1 mM DTT, 200 μM ATP, 2 U/ml inorganic pyrophosphatase (Sigma-Aldrich), 10 mM L-Pro (Sigma-Aldrich), 8 μM *P. falciparum* tRNApro, and 0.4 μM recombinant PRS. The aminoacylation reactions (55 μl total volume each) were performed in clear, flat-bottomed, 96-well plates (Costar 96-well standard microplates), and the reaction mixtures were incubated for 30 min at 37°C. Liberated inorganic phosphate was detected by addition of 15 μl of malachite green solution (Baykov et al., 1988) and incubated for 30 min at room temperature. Absorbance was measured at 621 nm using a Versa Max microplate reader. Reactions without enzyme or without L-Pro were performed as background controls, and data from reactions without L-Pro were subtracted from the measurements. For time-course experiments, 10 mM EDTA was added to the reaction mixture at different time points (0, 2, 5, 8, 10, 20, and 30 min) and mixed on ice to stop the reaction. For PRS inhibition, a reaction solution containing PRS (0.4 μM) was mixed with HF, FF, 6F-FF, and Th-FF at 0.1 nM to 10 μM in a 50-μl volume and incubated for 20 min at 37°C. Reactions were stopped as described above. All data are shown for three replicates as the mean ± SE.

Data Collection and Structure Determination

X-Ray diffraction data were collected at 100 K using Cu Kα radiation (λ = 1.54 Å) on an MAR345 image-plate detector mounted on a Rigaku MicroMax-007 rotating-anode X-ray generator. A total of 300 images were collected with 10 min exposure and 1° oscillation per frame. The diffraction images were processed and scaled with the HKL-2000 program suite. Structure was solved by molecular replacement in Phaser (McCoy et al., 2007) using the PfPRS-apo structure (Jain et al., 2014) (PDB code: 4TWA) as the template. There are two PfPRS-HF-AMPPNP complexes in the asymmetric unit with a solvent content of ~56%. The model was initially refined using REFMAC5 (Murshudov et al., 2011) and completed with phenix.refine in PHENIX (Adams et al., 2010). X-Ray refinement restraint parameters were generated for HF molecule using the Sketcher program in the CCP4 Suite (Winn et al., 2011). HF, AMPPNP, and water molecules were added into the electron density maps using COOT (Emsley and Cowtan, 2004). The quality of the final model and bound ligands was verified using composite simulated annealing omit maps. The occupancies of bound ligands and alternate conformations of protein residues were refined and confirmed using omit maps. Final model quality was analyzed using MolProbity (Chen et al., 2010), and the final model has 98% residues in favored regions and the remaining 2% residues in allowed regions of the Ramachandran plot. Statistics for data collection and structure refinement are given in Table 2. All structural superimposition and preparation of figures was done using UCSF Chimera (Pettersen et al., 2004) and PyMOL (http://www.pymol.org). The dimer interface buried surface area, hydrogen bonds, and salt bridges were analyzed using PISA (Krissinel and Henrick, 2007). Atomic coordinates and structural factors have been deposited into the PDB with accession code 4YDQ.

T. gondii Growth Inhibition

Methods and procedures for this section are available in the Supplemental Methods.

Analysis of Drug Cocktail on *P. falciparum* Growth

The isobologram method was used to evaluate the effects of co-administration of two tRNA synthetase inhibitors (HF and CL) as described previously (Loewe, 1953; Steel and Peckham, 1979). The concentrations of HF and CL required to reduce parasite growth by 50% (EC_{50}) were determined and plotted on the *x* and *y* axes in a two-coordinate plot. A straight line connecting these two 50% growth points (for the two drugs) corresponds to the line of additivity. Concentrations of HF and CL used in different combinations (*x*:*y*) were plotted. All points above the additivity line suggest antagonism between drugs and those below indicate synergism. In this case, experimental data points along the line indicate additive effects between the two drugs.

ACCESSION NUMBERS

Coordinates and structure factors for PfPRS-HF-AMPPNP have been deposited in the RCSB PDB under accession code 4YDQ.

SUPPLEMENTAL INFORMATION

Supplemental Information includes Supplemental Methods and one figure and can be found with this article online at http://dx.doi.org/10.1016/j.str.2015.02.011.

Table 2. Data Collection and Refinement Statistics

	PfPRS- HF- AMPPNP
Data Collection	
Space group	$P2_1$
Cell dimensions	
a, *b*, *c* (Å)	81.0, 88.9, 86.3
α, β, γ (°)	90, 96.7, 90
Resolution (Å)	50.0–2.3 (2.34–2.3)
R_{merge} (%)	0.090 (0.50)
$I/\sigma(I)$	21.2 (2.8)
Completeness (%)	99.5 (95.0)
Redundancy	5.8 (5.1)
Refinement	
Resolution	27.8–2.30 (2.36–2.30)
No. of reflections	51,322 (4,938)
R_{work}/R_{free} (%)	18.1/23.1
No. of atoms	
Protein	7,686
Ligand/ions	110/2
Water	291
B factor (Å^2)	
Protein	41.6
Ligand/ions	27.9/51.0
Water	37.0
RMSD	
Bond length (Å)	0.010
Bond angle (°)	1.275

Values in parentheses are for the highest-resolution shell.

AUTHOR CONTRIBUTIONS

V.J. performed purification of the enzyme, biochemical assays, and crystallization, and analyzed the data. V.J. and M.Y. collected X-ray data and determined the structure. B.T. and M.H. performed *Toxoplasma*-based assays. Y.O. and H.K. synthesized the FF derivatives. A.S. designed the study and participated in data analysis. All authors discussed the results and wrote the manuscript.

ACKNOWLEDGMENTS

This research was supported by DBT, Government of India OSRP grant PR6303 to A.S., and DBT grant PR3084 to A.S. and M.Y. V.J. is supported by a DBT Senior Research Fellowship. A.S. is additionally supported by the JC Bose fellowship. B.T. and M.A.H. are supported by the European Research Council (ERC Consolidator grant no. 614880 Hosting TOXO to M.A.H.).

Received: December 17, 2014
Revised: February 16, 2015
Accepted: February 22, 2015
Published: March 26, 2015

REFERENCES

Adams, P.D., Afonine, P.V., Bunkoczi, G., Chen, V.B., Davis, I.W., Echols, N., Headd, J.J., Hung, L.W., Kapral, G.J., Grosse-Kunstleve, R.W., et al. (2010). PHENIX: a comprehensive Python-based system for macromolecular structure solution. Acta Crystallogr. D Biol. Crystallogr. *66*, 213–221.

Baykov, A.A., Evtushenko, O.A., and Avaeva, S.M. (1988). A malachite green procedure for orthophosphate determination and its use in alkaline phosphatase-based enzyme immunoassay. Anal. Biochem. *171*, 266–270.

Bhatt, T.K., Kapil, C., Khan, S., Jairajpuri, M.A., Sharma, V., Santoni, D., Silvestrini, F., Pizzi, E., and Sharma, A. (2009). A genomic glimpse of aminoacyl-tRNA synthetases in malaria parasite *Plasmodium falciparum*. BMC Genomics *10*, 644.

Bhatt, T.K., Khan, S., Dwivedi, V.P., Banday, M.M., Sharma, A., Chandele, A., Camacho, N., Ribas de Pouplana, L., Wu, Y., Craig, A.G., et al. (2011). Malaria parasite tyrosyl-tRNA synthetase secretion triggers pro-inflammatory responses. Nat. Commun. *2*, 530.

Cestari, I., and Stuart, K. (2013). A spectrophotometric assay for quantitative measurement of aminoacyl-tRNA synthetase activity. J. Biomol. Screen. *18*, 490–497.

Chandra, B.R., Olivieri, A., Silvestrini, F., Alano, P., and Sharma, A. (2005). Biochemical characterization of the two nucleosome assembly proteins from *Plasmodium falciparum*. Mol. Biochem. Parasitol. *142*, 237–247.

Chen, V.B., Arendall, W.B., 3rd, Headd, J.J., Keedy, D.A., Immormino, R.M., Kapral, G.J., Murray, L.W., Richardson, J.S., and Richardson, D.C. (2010). MolProbity: all-atom structure validation for macromolecular crystallography. Acta Crystallogr. D Biol. Crystallogr. *66*, 12–21.

Coatney, G.R., Cooper, W.C., Culwell, W.B., White, W.C., and Imboden, C.A., Jr. (1950). Studies in human malaria. XXV. Trial of febrifugine, an alkaloid obtained from *Dichroa febrifuga* Lour., against the Chesson strain of *Plasmodium vivax*. J. Natl. Malar. Soc. *9*, 183–186.

Derbyshire, E.R., Mazitschek, R., and Clardy, J. (2012). Characterization of *Plasmodium* liver stage inhibition by halofuginone. ChemMedChem *7*, 844–849.

Elkin, M., Ariel, I., Miao, H.Q., Nagler, A., Pines, M., de-Groot, N., Hochberg, A., and Vlodavsky, I. (1999). Inhibition of bladder carcinoma angiogenesis, stromal support, and tumor growth by halofuginone. Cancer Res. *59*, 4111–4118.

Emsley, P., and Cowtan, K. (2004). Coot: model-building tools for molecular graphics. Acta Crystallogr. D Biol. Crystallogr. *60*, 2126–2132.

Geary, T.G., Divo, A.A., and Jensen, J.B. (1983). An in vitro assay system for the identification of potential antimalarial drugs. J. Parasitol. *69*, 577–583.

Gill, J., Yogavel, M., Kumar, A., Belrhali, H., Jain, S.K., Rug, M., Brown, M., Maier, A.G., and Sharma, A. (2009). Crystal structure of malaria parasite nucleosome assembly protein: distinct modes of protein localization and histone recognition. J. Biol. Chem. *284*, 10076–10087.

Halevy, O., Nagler, A., Levi-Schaffer, F., Genina, O., and Pines, M. (1996). Inhibition of collagen type I synthesis by skin fibroblasts of graft versus host disease and scleroderma patients: effect of halofuginone. Biochemical Pharmacol. *52*, 1057–1063.

Hewitt, R.I., Wallace, W.S., Gill, E.R., and Williams, J.H. (1952). An antimalarial alkaloid from Hydrangea. XIII. The effects of various synthetic quinazolones against *Plasmodium lophurae* in ducks. Am. J. Trop. Med. Hyg. *1*, 768–772.

Hoen, R., Novoa, E.M., Lopez, A., Camacho, N., Cubells, L., Vieira, P., Santos, M., Marin-Garcia, P., Bautista, J.M., Cortes, A., et al. (2013). Selective inhibition of an apicoplastic aminoacyl-tRNA synthetase from *Plasmodium falciparum*. ChemBioChem *14*, 499–509.

Hoepfner, D., McNamara, C.W., Lim, C.S., Studer, C., Riedl, R., Aust, T., McCormack, S.L., Plouffe, D.M., Meister, S., Schuierer, S., et al. (2012). Selective and specific inhibition of the *Plasmodium falciparum* lysyl-tRNA synthetase by the fungal secondary metabolite cladosporin. Cell Host Microbe *11*, 654–663.

Ibba, M., and Soll, D. (2000). Aminoacyl-tRNA synthesis. Annu. Rev. Biochem. *69*, 617–650.

Istvan, E.S., Dharia, N.V., Bopp, S.E., Gluzman, I., Winzeler, E.A., and Goldberg, D.E. (2011). Validation of isoleucine utilization targets in *Plasmodium falciparum*. Proc. Natl. Acad. Sci. USA *108*, 1627–1632.

Jackson, K.E., Habib, S., Frugier, M., Hoen, R., Khan, S., Pham, J.S., Ribas de Pouplana, L., Royo, M., Santos, M.A., Sharma, A., et al. (2011). Protein translation in *Plasmodium* parasites. Trends Parasitol. *27*, 467–476.

Jain, V., Kikuchi, H., Oshima, Y., Sharma, A., and Yogavel, M. (2014). Structural and functional analysis of the anti-malarial drug target prolyl-tRNA synthetase. J. Struct. Funct. Genomics *15*, 181–190.

Keller, T.L., Zocco, D., Sundrud, M.S., Hendrick, M., Edenius, M., Yum, J., Kim, Y.J., Lee, H.K., Cortese, J.F., Wirth, D.F., et al. (2012). Halofuginone and other febrifugine derivatives inhibit prolyl-tRNA synthetase. Nat. Chem. Biol. *8*, 311–317.

Khan, S., Sharma, A., Jamwal, A., Sharma, V., Pole, A.K., Thakur, K.K., and Sharma, A. (2011). Uneven spread of cis- and trans-editing aminoacyl-tRNA synthetase domains within translational compartments of *P. falciparum*. Sci. Rep. *1*, 188.

Khan, S., Garg, A., Camacho, N., Van Rooyen, J., Kumar Pole, A., Belrhali, H., Ribas de Pouplana, L., Sharma, V., and Sharma, A. (2013a). Structural analysis of malaria-parasite lysyl-tRNA synthetase provides a platform for drug development. Acta Crystallogr. D Biol. Crystallogr. *69*, 785–795.

Khan, S., Garg, A., Sharma, A., Camacho, N., Picchioni, D., Saint-Leger, A., Ribas de Pouplana, L., Yogavel, M., and Sharma, A. (2013b). An appended domain results in an unusual architecture for malaria parasite tryptophanyl-tRNA synthetase. PLoS One *8*, e66224.

Khan, S., Sharma, A., Belrhali, H., Yogavel, M., and Sharma, A. (2014). Structural basis of malaria parasite lysyl-tRNA synthetase inhibition by cladosporin. J. Struct. Funct. Genomics *15*, 63–71.

Kikuchi, H., Yamamoto, K., Horoiwa, S., Hirai, S., Kasahara, R., Hariguchi, N., Matsumoto, M., and Oshima, Y. (2006). Exploration of a new type of antimalarial compounds based on febrifugine. J. Med. Chem. *49*, 4698–4706.

Kikuchi, H., Horoiwa, S., Kasahara, R., Hariguchi, N., Matsumoto, M., and Oshima, Y. (2014). Synthesis of febrifugine derivatives and development of an effective and safe tetrahydroquinazoline-type antimalarial. Eur. J. Med. Chem. *76*, 10–19.

Koepfli, J.B., Mead, J.F., and Brockman, J.A., Jr. (1947). An alkaloid with high antimalarial activity from *Dichroa febrifuga*. J. Am. Chem. Soc. *69*, 1837.

Koh, C.Y., Kim, J.E., Shibata, S., Ranade, R.M., Yu, M., Liu, J., Gillespie, J.R., Buckner, F.S., Verlinde, C.L., Fan, E., et al. (2012). Distinct states of methionyl-tRNA synthetase indicate inhibitor binding by conformational selection. Structure *20*, 1681–1691.

Krissinel, E., and Henrick, K. (2007). Inference of macromolecular assemblies from crystalline state. J. Mol. Biol. *372*, 774–797.

Linder, M.R., Heckeroth, A.R., Najdrowski, M., Daugschies, A., Schollmeyer, D., and Miculka, C. (2007). (2R,3S)-(+)- and (2S,3R)-(-)-halofuginone lactate: synthesis, absolute configuration, and activity against *Cryptosporidium parvum*. Bioorg. Med. Chem. Lett. *17*, 4140–4143.

Loewe, S. (1953). The problem of synergism and antagonism of combined drugs. Arzneimittelforschung *3*, 285–290.

Matulis, D., Kranz, J.K., Salemme, F.R., and Todd, M.J. (2005). Thermodynamic stability of carbonic anhydrase: measurements of binding affinity and stoichiometry using ThermoFluor. Biochemistry *44*, 5258–5266.

McCoy, A.J., Grosse-Kunstleve, R.W., Adams, P.D., Winn, M.D., Storoni, L.C., and Read, R.J. (2007). Phaser crystallographic software. J. Appl. Crystallogr. *40*, 658–674.

McGaha, T., Kodera, T., Phelps, R., Spiera, H., Pines, M., and Bona, C. (2002). Effect of halofuginone on the development of tight skin (TSK) syndrome. Autoimmunity *35*, 277–282.

Murshudov, G.N., Skubak, P., Lebedev, A.A., Pannu, N.S., Steiner, R.A., Nicholls, R.A., Winn, M.D., Long, F., and Vagin, A.A. (2011). REFMAC5 for the refinement of macromolecular crystal structures. Acta Crystallogr. D Biol. Crystallogr. *67*, 355–367.

Navadgi, V.M., Chandra, B.R., Mishra, P.C., and Sharma, A. (2006). The two *Plasmodium falciparum* nucleosome assembly proteins play distinct roles in histone transport and chromatin assembly. J. Biol. Chem. *281*, 16978–16984.

Pettersen, E.F., Goddard, T.D., Huang, C.C., Couch, G.S., Greenblatt, D.M., Meng, E.C., and Ferrin, T.E. (2004). UCSF Chimera—a visualization system for exploratory research and analysis. J. Comput. Chem. *25*, 1605–1612.

Pham, J.S., Dawson, K.L., Jackson, K.E., Lim, E.E., Pasaje, C.F., Turner, K.E., and Ralph, S.A. (2014). Aminoacyl-tRNA synthetases as drug targets in eukaryotic parasites. Int. J. Parasitol. Drugs Drug Resist. *4*, 1–13.

Pines, M., and Nagler, A. (1998). Halofuginone: a novel antifibrotic therapy. Gen. Pharmacol. *30*, 445–450.

Pines, M., Snyder, D., Yarkoni, S., and Nagler, A. (2003). Halofuginone to treat fibrosis in chronic graft-versus-host disease and scleroderma. Biol. Blood Marrow Transplant. *9*, 417–425.

Ryley, J.F., and Betts, M.J. (1973). Chemotherapy of chicken coccidiosis. Adv. Pharmacol. Chemother. *11*, 221–293.

Ryley, J.F., and Wilson, R.G. (1975). Laboratory studies with some recent anticoccidials. Parasitology *70*, 203–222.

Sharma, A., and Sharma, A. (2011). Fatty acid induced remodeling within the human liver fatty acid-binding protein. J. Biol. Chem. *286*, 31924–31928.

Sharma, A., Yogavel, M., Akhouri, R.R., Gill, J., and Sharma, A. (2008). Crystal structure of soluble domain of malaria sporozoite protein UIS3 in complex with lipid. J. Biol. Chem. *283*, 24077–24088.

Smilkstein, M., Sriwilaijaroen, N., Kelly, J.X., Wilairat, P., and Riscoe, M. (2004). Simple and inexpensive fluorescence-based technique for high-throughput antimalarial drug screening. Antimicrob. Agents Chemother. *48*, 1803–1806.

Son, J., Lee, E.H., Park, M., Kim, J.H., Kim, J., Kim, S., Jeon, Y.H., and Hwang, K.Y. (2013). Conformational changes in human prolyl-tRNA synthetase upon binding of the substrates proline and ATP and the inhibitor halofuginone. Acta Crystallogr. D Biol. Crystallogr. *69*, 2136–2145.

Steel, G.G., and Peckham, M.J. (1979). Exploitable mechanisms in combined radiotherapy-chemotherapy: the concept of additivity. Int. J. Radiat. Oncol. Biol. Phys. *5*, 85–91.

Tonkin, C.J., van Dooren, G.G., Spurck, T.P., Struck, N.S., Good, R.T., Handman, E., Cowman, A.F., and McFadden, G.I. (2004). Localization of organellar proteins in *Plasmodium falciparum* using a novel set of transfection vectors and a new immunofluorescence fixation method. Mol. Biochem. Parasitol. *137*, 13–21.

Trager, W., and Jensen, J.B. (2005). Human malaria parasites in continuous culture. J. Parasitol. *91*, 484–486.

Winn, M.D., Ballard, C.C., Cowtan, K.D., Dodson, E.J., Emsley, P., Evans, P.R., Keegan, R.M., Krissinel, E.B., Leslie, A.G., McCoy, A., et al. (2011). Overview of the CCP4 suite and current developments. Acta Crystallogr. D Biol. Crystallogr. *67*, 235–242.

Zhou, H., Sun, L., Yang, X.L., and Schimmel, P. (2013). ATP-directed capture of bioactive herbal-based medicine on human tRNA synthetase. Nature *494*, 121–124.